HHS Public Access

Author manuscript

Contrast Media Mol Imaging. Author manuscript; available in PMC 2016 May 25.

Published in final edited form as:

Contrast Media Mol Imaging. 2011 ; 6(4): 219–228. doi:10.1002/cmmi.421.

A self-calibrating PARACEST MRI contrast agent that detects esterase enzyme activity

Yuguo Li[a], **Vipul R. Sheth**[b], **Guanshu Liu**[c], and **Mark D. Pagel**[a,d,*]

[a]Department of Biomedical Engineering, University of Arizona, Tucson, AZ, USA

[b]Department of Biomedical Engineering, Case Western Reserve University, Cleveland, OH, USA

[c]Department of Radiology, Johns Hopkins University, Baltimore, MD, USA

[d]Department of Chemistry and Biochemistry, University of Arizona, Tucson, AZ, USA

Abstract

The CEST effect of many PARACEST MRI contrast agents changes in response to a molecular biomarker. However, other molecular biomarkers or environmental factors can influence CEST, so that a change in CEST is not conclusive proof for detecting the biomarker. To overcome this problem, a second control CEST effect may be included in the same PARACEST agent, which is responsive to all factors that alter the first CEST effect except for the biomarker to be measured. To investigate this approach, a PARACEST MRI contrast agent was developed with one CEST effect that is responsive to esterase enzyme activity and a second control CEST effect. The ratio of the two CEST effects was independent of concentration and T_1 relaxation, so that this agent was self-calibrating with respect to these factors. This ratiometric method was dependent on temperature and was influenced by MR coalescence as the chemical exchange rates approached the chemical shifts of the exchangable protons as temperature was increased. The two CEST effects also showed evidence of having different pH dependencies, so that this agent was not self-calibrating with respect to pH. Therefore, a self-calibrating PARACEST MRI contrast agent can more accurately detect a molecular biomarker such as esterase enzyme activity, as long as temperature and pH are within an acceptable physiological range and remain constant.

Keywords

PARACEST; MRI; contrast agent; esterase; enzyme activity

1. Introduction

MRI contrast agents that are detected through PARAmagnetic Chemical Exchange Saturation Transfer (PARACEST) have provided new capabilities for molecular imaging (1). The CEST effect increases with an increasing chemical exchange rate of transferring a proton between the contrast agent and water [eqns (1) and (2)]. The CEST effect decreases if the exchange rate approaches the chemical shift of the agent's exchangeable proton (defined

*Correspondence to: M. D. Pagel, Department of Biomedical Engineering and Chemistry and Biochemistry, Arizona Cancer Center, room 4949, University of Arizona, Tucson, AZ 85724-5024, USA. ; Email: mpagel@u.arizona.edu

as the MR frequency of the exchangeable proton relative to the MR frequency of water, following the convention used for MRI studies) due to coalescence of the chemical shifts of water and the agent's exchangeable proton. The exchange rate is dictated by the type of chemical group that has an exchangeable proton on the agent, and is influenced by the electronic and steric properties of other chemical groups on the agent in addition to environmental conditions such as temperature and pH. Therefore, responsive PARACEST agents show altered CEST effects when their chemical exchange rates are altered by enzymes or metabolites that change chemical groups, ions or metabolites that change ligand properties, or changes in pH or temperature (Eqns. 1 and 2).

$$\%\,\mathrm{CEST}=1-\frac{M_{\mathrm{s}}}{M_0} \quad (1)$$

$$\frac{M_s}{M_0}=\frac{1}{1+\frac{n_{\mathrm{CA}}[\mathrm{CA}]T_{1\mathrm{sat}}k_{ex}}{n_{\mathrm{H_2O}}[\mathrm{H_2O}]}} \quad (2)$$

where M_s is the water MR signal amplitude with selective saturation at the MR frequency of the CEST agent; M_0 is the water MR signal amplitude with selective saturation at the MR frequency at the opposite chemical shift relative to 0 ppm as compard with the MR frequency of the CEST agent; n_{H2O} and n_{CA} are the number of exchangeable protons on a water molecule and the chemical group of the contrast agent, respectively; [H_2O] and [CA] are the concentration of water and the saturated contrast agent, respectively; k_{ex} is the chemical exchange rate for exchanging a proton on a PARACEST agent with a proton on a water molecule; and T_{1sat} is the longitudinal MR relaxation time of the sample with the contrast agent and in the presence of selective saturation.

Multiple factors can alter the chemical exchange rate of a PARACEST agent, so that the change in CEST cannot be conclusively assigned to a single factor during molecular imaging studies (3). The influence of temperature and pH are especially problematic for studies of enzyme activities, ions and metabolites, because temperature and pH are omnipresent in all molecular imaging studies. Furthermore, other conditions such as the endogenous T_1 relaxation time and the concentration of the agent can change the magnitude of the detected CEST effect. Therefore, interpreting the change of a single CEST effect is a daunting challenge.

To overcome this problem, PARACEST molecular imaging studies have been designed to include a second CEST effect as a control. This second CEST effect is designed to be responsive to all factors as the first CEST effect, except for the molecular change to be measured. The ratio of the CEST effects can then more conclusively measure the intended target or factor of the molecular imaging study. This approach has been investigated with two PARACEST agents, each with a single CEST effect, in order to improve the accuracy of measuring enzyme activities, metabolites or pH (4–7). Because two PARACEST agents may have different pharmacokinetics during *in vivo* studies, a single PARACEST agent with two CEST effects has been developed to more accurately measure pH (8).

The study described in this report investigated whether the use of two CEST effects from one PARACEST MRI contrast agent can more definitively detect enzyme activity. The first previously reported example of an enzyme-responsive PARACEST agent relied on the disappearance of a single CEST effect when caspase-3 converted an amide to an amine (9). This approach was improved by relying on the appearance of a single CEST effect when *β*-galactosidase catalyzed the conversion of a carbamate to an amine (10). This improved approach also used a modular chemical design that connected a PARACEST contrast agent to a substrate using a spontaneously disassembling spacer. Our study used the same modular design concept by connecting a PARACEST contrast agent to an ester group using a spontaneously disassembling tri-methyl lock (TML) spacer (Fig. 1) (11). After the ester is cleaved by an esterase enzyme, the tri-methyl lock moiety has unfavorable steric interactions between three methyl groups that encourage rapid lactonization to form a hydrocoumarin. As a byproduct of this lactonization, an amide is converted to an amine that can generate a CEST effect. This PARACEST agent contains a second amide group, which can produce a second control CEST effect that is not responsive to enzyme activity but is responsive to all other factors that influence the first CEST effect. Thus, a ratio of the responsive and control CEST effects may more definitively report on enzyme activity as compared with previous enzyme-responsive PARACEST agents. We refer to this type of PARACEST agent with responsive and control CEST effects as a ‘self-calibrating’ PARACEST agent.

2. Results

2.1. Synthesis of the PARACEST MRI contrast agent

The PARACEST MRI contrast agent, Yb-DO3A-oAA-TML-ester, consists of two modular moieties, Yb-DO3A-oAA and TML-ester (Fig. 2). DO3A-oAA was synthesized by acylating *o*-nitroaniline, coupling this product to 1,4,7,10-tetraazacyclododecane-1,4,7-triacetic acid (DO3A), and reducing the nitrobenzene via hydrogenation. This product was then used to chelate Yb(III) to form Yb-DO3A-oAA. TML-ester was synthesized using a previously reported method, and then coupled to Yb-DO3A-oAA via an amide bond using a carbodiimide (7,11). Care was taken to use pure reactants and clean glassware in order to avoid contamination from environmental esterases. This coupling was conducted in DMF to accommodate the hydrophobic TML-ester and the hydrophilic Yb-DO3A-oAA, resulting in a 38% yield of pure product. The final product showed a stable CEST effect for at least three days, which demonstrated that the agent was a stable compound.

2.2. Detection of esterase enzyme activity

All analyses of CEST effects were conducted by recording CEST spectra that represent the water signal amplitude after selectively saturating each MR frequency in 1 ppm increments ranging between +30 and −30 ppm (Fig. 3). The CEST effect is commonly measured by comparing the water signal amplitude after selective saturation at the chemical shift of the CEST agent’s exchangeable proton (M_s) with the water signal amplitude at the opposite chemical shift relative to 0 ppm (M_0). However, because the chemical shifts of M_s for the amine and amide of Yb-DO3A-oAA occur at +12 and −10 ppm, M_0 cannot be measured at −12 and +10 ppm without influence from the other CEST effect. To overcome this problem, the CEST spectra were fit to a single function that consisted of a sum of three Lorentzian line shapes (Fig. 4) (12). The amplitudes of the Lorentzian lines initially centered at +12 and −10 ppm were used to determine M_s for each CEST effect, and the Lorentzian line initially centered at 0 ppm was used to determine M_0 for each CEST effect. As an additional benefit, this fitting procedure accounted for small changes in chemical shifts that were caused by changes in temperature.

A 20 mM sample of Yb-DO3A-oAA-TML-ester at pH 7.2 and 37 °C showed a 10.2% CEST effect at −10.6 ppm (Fig. 3A). This CEST effect was assigned to the amide that was closest to the lanthanide ion, based on CEST studies of similar Yb(III) chelates with amides at the same structural position (5). A CEST effect was not observed from the responsive amide that forms the connection to the TML-ester moiety. After adding pig liver esterase and waiting for 24 h at 25 °C, the solution was heated to 37 °C and showed two CEST effects with magnitudes of 8.5 and 3.0% at −10.5 and +12.0 ppm, respectively. Subsequent mass spectral analysis of the solution confirmed that the PARACEST agent was converted to a hydrocoumarin and Yb-DO3A-oAA. The appearance of the new CEST effect at 12 ppm was assigned to the amine of Yb-DO3A-oAA and the CEST effect at −10.5 ppm was assigned to the amide of this product, based on the CEST effect of the amide prior to cleavage (which is anticipated to be observed at the same chemical shift after cleavage) and similar results reported for Yb-DO3A-oAA (7).

A similar study was conducted to detect esterase enzyme activity in cell culture medium (Fig. 3B). The medium was collected after incubation for 24 h with *P. aeruginosa*, which are known to express esterase enzymes (13). Yb-DO3A-oAA-TML-ester was added to this medium to create a 20 mM solution of this PARACEST agent, which showed a 12.6% CEST effect at −10.7 ppm at 37 °C. After waiting for 24 h at 25 °C, the sample was heated to 37 °C and showed two CEST effects with magnitudes of 8.7 and 5.8% at −10.3 and +12.2 ppm that were assigned to the amide and amine, respectively. This study was repeated with cell culture medium that was autoclaved prior to adding the PARACEST agent. No change in the CEST spectrum was observed with this autoclaved medium (data not shown), indicating that reaction in the unautoclaved medium occurred due to biological activity and not due to chemical instability of the agent in the medium.

2.3. T_1 relaxation

The remaining studies compared the MR properties of the responsive amine and control amide of Yb-DO3A-oAA. The r_{1sat} relaxivities of the contrast agent was measured with selective saturation applied at +12 and −10 ppm, and the r_1 relaxivity was measured with saturation applied at +80 ppm and with no selective saturation (Table 1, Fig. 5A, Eqn. 3). These results showed that the r_{1sat} values were almost identical during selective saturation of the amine and amide, as the amine-to-amide ratio of these r_{1sat} relaxivities was 1.087. This ratio supports the hypothesis that the control amide can account for the T_{1sat} relaxation of the responsive amine. These r_{1sat} relaxivities were greater than the r_1 relaxivities during selective saturation at +80 ppm or with no saturation, which confirmed that T_{1sat} relaxation of CEST agents must be assessed in the presence of selective saturation (14). In all cases, the y-intercept of the relaxivity plots was 0.237 s^{-1}, indicating that the T_1 relaxation time of the water without agent was 4.22 s.

$$R_{1sat}=T_{1sat}^{-1}=T_{1W}^{-1}+r_{1sat}[\mathrm{CA}] \quad (3a)$$

$$R_{1}=T_{1}^{-1}=T_{1W}^{-1}+r_{1}[\mathrm{CA}] \quad (3b)$$

where T_{1W} is the longitudinal MR relaxation time of water without contrast agent; T_1 is the longitudinal MR relaxation time of the sample without selective saturation of the agent; r_{1sat} is the r_1 relaxivity of the contrast agent with a saturated contrast agent; and r_1 is the r_1 relaxivity of the contrast agent without selective saturation of the agent.

The T_{1sat} relaxation times were also studied with respect to temperature, which can be approximated to be a linear function for the temperatures and MR frequencies used in this study (Fig. 5B) (15). Selective saturation of the amine caused a temperature-dependent change in T_{1sat} relaxation time of 0.019 s °C^{-1} while selective saturation of the amide showed a measurement of 0.025 s °C^{-1}. The temperature-dependent change in the ratio of these T_{1sat} relaxation times was 0.0024s °C^{-1}. Therefore, a ratiometric comparison of T_{1sat} relaxation times was almost constant with respect to temperature, indicating that the control amide can be used to account for the T_{1sat} relaxation of the responsive amine throughout a wide range of temperatures.

2.4. CEST and concentration

The CEST effects of the amine and the amide of Yb-DO3A-oAA each increased with increasing concentration (Fig. 6A). Each CEST effect matched the behavior of a CEST–concentration calibration that follows a two-pool model in which the two pools are water and one type of exchangeable proton on the agent (16). Therefore, the presence of the amide on the amine–water exchange process, and the presence of the amine on the amide–water exchange process, had negligible influences and a three-pool model was not needed for this analysis. The average ratio of the amine-to-amide CEST effects at each concentration is 0.72. Yet this ratio of the CEST effects is constant with respect to concentration, so that the control amide can account for the concentration of the responsive amine.

A Hanes CEST–concentration calibration, which can be derived from eqns (1) and (2), was used for this analysis because this type of linear calibration is very accurate at low concentrations [Fig. 6B, eqn (4)] (3). The Hanes calibration is more accurate than the Lineweaver–Burke CEST–concentration calibration that we have previously reported (7). Furthermore, the Hanes calibration separates the conditions of T_1 relaxivity (r_1) and chemical exchange rate (k_{ex}) for a CEST agent. The slope of this calibration, $-r_{1sat}T_{1w}$, was slightly lower than $-r_{1sat}T_{1w}$ determined from T_1 relaxation analysis for both the amine and the amide (Table 1). The ratio of the amine-to-amide slopes of the Hanes calibration matched the ratio of the r_{1sat} relaxivities indicating that the small difference in this comparison of CEST and T_1 relaxation is due to a small inaccuracy in determining T_{1W} from the T_1 relaxation analysis. This ratio of the slopes of the Hanes calibrations of CEST results further supports the hypothesis that the control amide can account for the T_{1sat} relaxation of the responsive amine.

$$\frac{\left(\frac{M_0}{M_S}-1\right)}{[\mathrm{CA}]}=\frac{n_{\mathrm{CA}}\,T_{1\mathrm{W}}k_{\mathrm{ex}}}{n_{\mathrm{H_2O}}[\mathrm{H_2O}]}-r_{1\mathrm{sat}}\,T_{1\mathrm{W}}\left(\frac{M_0}{M_S}-1\right) \quad (4)$$

The y-intercept of the Hanes calibration includes the chemical exchange rate, which was determined to be 93 and 375 Hz for the amine and amide, respectively. The chemical exchange rate of an amine is typically ~3000 Hz (17). Our previous report indicated that a hydrogen bond may form between the amine and an adjacent acetate ligand of this agent, which may slow this exchange rate (7). Because the pK_a of an amine and amide are typically much higher than the pH of 7.2 used in this study, the amine has three exchangeable protons and the amide has one exchangeable proton (17). The ratio of the total chemical exchange rates, $n_{CA}k_{ex}$, was 0.74, which was very similar to the average ratio of the amine-to-amide CEST effects at each concentration. Therefore, the difference between the responsive and control CEST effects can be entirely attributed to the difference in total chemical exchange processes for each chemical group.

2.5. CEST and T_1 relaxation

The CEST effects of Yb-DO3A-oAA were studied with respect to T_{1W} relaxation time by serially doping a sample of the agent with gadodiamide. The value of T_{1W} for each doped sample was determined by measuring the T_1 relaxation time of the sample and then using eqn (3b) to remove the contribution of T_1 relaxation of the PARACEST agent. The amine-to-amide ratio of the CEST effects was much less dependent on T_{1sat} (slope = − 0.19% s^{-1}) relative to the CEST effect of the amine (slope = 3.23% s^{-1}) and amide (slope = 4.17% s^{-1}), showing that the CEST ratio is self-calibrating with respect to T_{1W} relaxation.

The detected CEST effects were also evaluated using a modification of the Hanes calibration and the r_{1sat} relaxivities reported above [eqn (5)]. The slope of this calibration was used to determine the concentration of saturated contrast agent, and the y-intercept was used to determine the chemical exchange rate (Fig. 7). The precisions of these analyses were poor, as evidenced by poor linear correlation coefficients, so that these results should be considered qualitative rather than quantitative. The chemical exchange rates of 82 and 355 Hz for the amine and amide, respectively, were qualitatively close the values of the exchange rates that were determined from the CEST dependence on concentration. The concentration of contrast agent when the amide or amine was saturated was determined to be 10.3 and 16.8 mM, respectively, which is less than the 20 mM concentration of contrast agent in the sample, indicating that saturation of the amine and the amide was incomplete. This incomplete saturation was attributed to a chemical exchange rate that is non-negligible relative to the chemical shift, which results in chemical shift coalescence. The amine experienced more saturation than the amide because the chemical exchange rate is lower and the chemical shift is higher for the amine relative to the amide.

$$\frac{\left(\frac{M_0}{M_s}-1\right)}{T_{1\mathrm{W}}}=\frac{n_{\mathrm{CA}}[\mathrm{CA}]k_{\mathrm{ex}}}{n_{\mathrm{H_2O}}[\mathrm{H_2O}]}-r_{1\mathrm{sat}}[\mathrm{CA}]\left(\frac{M_0}{M_s}-1\right) \quad (5)$$

2.6. CEST and temperature

The CEST effect of the amide increased to a maximum at 27.2 °C, and then decreased at higher temperatures (Fig. 8A). This result differed from our previous report of temperature dependence of Yb-DO3A-oAA (7). Our previous result measured the CEST effects at a single chemical shift, and our more recent result measured the CEST effect while allowing for a variable chemical shift. Our latter approach is more accurate for evaluating a temperature-dependent CEST effect because the chemical shift of the CEST effect changes with temperature (Fig. 8B). The width of the amide's CEST effect continuously increased with increasing temperature (Fig. 8C), which indicated that the chemical exchange rate increased with increasing temperature and could not explain the decrease in CEST effect. This decrease in the CEST effect was attributed to a chemical exchange rate that approaches the chemical shift, which results in chemical shift coalescence and incomplete saturation. Similarly, heating the sample increased the CEST effect of the amine until this effect plateaued at the highest-studied temperatures, showing that the amine's chemical exchange rate becomes non-negligible relative to the chemical shift at high temperatures. This behavior occurs at a higher temperature for the amine than for the amide because the chemical exchange rate is lower and the chemical shift is higher for the amine relative to the amide. This result indicates that a simplistic comparison of the control CEST effect and responsive CEST effect may still detect enzyme activity as long as the temperature remains constant.

A more sophisticated analysis can be performed if CEST is considered to be a reaction that converts a water molecule reactant with unsaturated protons to a product with one saturated proton (Fig. 9A). If the PARACEST agent is immediately saturated after accepting an unsaturated proton from water, then the PARACEST agent acts as a catalyst because the form of the agent does not change before and after the reaction (3). The CEST reaction has just one water molecule reactant and is therefore a first-order reaction with a temperature dependence that is described by the Arrhenius equation [eqn (6)]. This equation can be combined with the equation for a two-pool model [eqn (2)] to create a linear relationship that includes the ratio of the CEST effects and the inverse of temperature [eqn (7)]. The plot of experimental data that matches this equation is linear between 27.2 and 53.2 °C (r^2 = 0.988) (Fig. 9B).

The CEST–T_1 relaxation analysis and the decreasing CEST effect of the amide with increasing temperature indicates incomplete saturation of the amine and amide. Yet the linear plot of eqn (7) indicates that the ratio of the concentrations of saturated amine and amide is constant between 27.2 and 53.2 °C. A potential pitfall of this analysis method is the use of logarithmic functions that temper the appearance of non-linearity, which reduces the sensitivity of this method to variances in the ratio of concentrations of the saturated amine and amide. Still, this more sophisticated analysis provides qualitative evidence that the control amide can be used to account for the temperature dependence of the responsive amine's CEST effect, especially through the limited range of relevant physiological temperatures.

$$k_{\mathrm{ex}}=A\mathrm{e}^{-Ea/RT} \quad (6)$$

where A is the Arrhenius prefactor; E_a is the activation energy; R is the molar gas constant; and T is the temperature.

$$\ln\left\{\frac{\left(\frac{M_0}{M_s}-1\right)_{\mathrm{amine}}}{\left(\frac{M_0}{M_s}-1\right)_{\mathrm{amide}}}\right\}=\frac{(E_{\mathrm{a,amide}}-E_{\mathrm{a,amine}})\ln\left\{\frac{(n_{\mathrm{CA}}A[\mathrm{CA}])_{\mathrm{amine}}}{(n_{\mathrm{CA}}A[\mathrm{CA}])_{\mathrm{amine}}}\right\}}{RT} \quad (7)$$

3. Discussion

Both the hydrophilic Yb-DO3A-oAA and hydrophobic TML-ester were not soluble in most solvents, but both were sufficiently soluble in dimethylformamide. The condensation of these reactants resulted in a low coupling yield, presumably due to steric constraints in the trimethyl lock substrate and the low nucleophilicity of the aromatic amine. The chelation of Yb(III) with DO3A-oAA was performed prior to coupling this metal chelate to TML-ester because TML-ester is unstable at high temperatures that are typically used to accelerate the chelation process. Despite these limitations, a sufficient amount of pure product was synthesized for subsequent studies.

The PARACEST agent showed the appearance of a CEST effect from the responsive amine after esterase was added to the sample. Similarly, this CEST effect also appeared after the agent was added to unautoclaved cell culture medium that contained extracellular esterases expressed by *P. aeruginosa*. The ratio of the CEST effects changed from 0 before esterase catalysis to 36 and 66% after esterase catalysis in the enzyme solution and cell culture medium, respectively, which demonstrated that the ratiometric approach can detect esterase activity. Although both samples were buffered, de-esterification of 20 mM of the PARACEST agent produced 20 mM of hydrogen ions that likely caused a small decrease in pH. Because chemical exchange of an amine or amide is base-catalyzed, the chemical exchange rates are expected to decrease at lower pH (17). As expected, the CEST effect of the control amide decreased after enzyme catalysis. The amine-to-amide ratio of the CEST effects after catalysis was also lower than the same ratio measured in other studies at higher pH, indicating that the drop in pH decreased the chemical exchange rate of the amine to a greater extent than the amide.

The $r_{1\mathrm{sat}}$ relaxivities of the agent in the presence of selective saturations at +12 and −10 ppm are not negligible, and the $T_{1\mathrm{W}}$ relaxation time of the water is dependent on temperature. However, T_1 relaxation is almost identical for the responsive amine and the control amide. Similarly, the CEST effects of the amine and the amide of Yb-DO3A-oAA showed a strong dependence on concentration, but the ratio of these CEST effects showed a negligible dependence on concentration. Therefore, the ratio of CEST from the responsive amine and the control amide is independent of concentration and T_1 relaxation, so that this agent is self-calibrating with regard to these factors.

A fundamental tenet of CEST studies is the requirement that the chemical exchange rate be less than the chemical shift. This study demonstrates the chemical exchange rates that are less than the chemical shift still strongly influence the CEST effect if the exchange rate is sufficiently high to cause some MR coalescence that leads to incomplete saturation. A similar conclusion was previously reported by comparing a related analytical method with a numerical solution to the Bloch equations that included chemical exchange (18). This comparison showed that the analytical method underestimates high chemical exchange rates due to incomplete saturation. Therefore, the ratiometric comparison of the two CEST effects is simplified if the CEST MRI study is conducted at constant temperature. Yet the concentration ratio of saturated amine and saturated amide was constant between 27.2 and 53.2 °C, so that the control amide can account for the incomplete saturation of the responsive amine within this temperature range using a more sophisticated analysis. As shown in the study of the enzyme reaction and in other CEST studies, pH also affects chemical exchange rates so that this ratiometric CEST method should be conducted with constant pH. Furthermore, if this contrast agent is to be used for accurate quantification of enzyme activity (rather than the detection of enzyme activity shown in this report), then the temperature and pH should be determined to accurately account for their influences on the CEST effects. Although changes in pH or temperature may change the conformation of the contrast agent, the smooth changes in each CEST effect with respect to pH and temperature indicate that possible conformational changes are gradual and not abrupt transitions. Fortunately, the two CEST effects are similar in magnitude at physiological pH and temperature, which facilitates a precise measurement of this ratio.

The Hanes calibration [eqn (4)] provides a method for determining the r_{1sat} relaxivity and the chemical exchange rate if T_{1W} and concentration are known. A modification of the Hanes calibration [eqn (5)] provides a method for determining the concentration of a saturated PARACEST agent and the chemical exchange rate if T_{1W} and the r_{1sat} relaxivity are known. Importantly, this second method can determine the concentration of the saturated PARACEST agent, which may be less than the total concentration of the agent. Although these linear graphical methods are convenient, a more rigorous analysis is needed to evaluate the precision and accuracy of these methods, and to compare these methods with other MR methods that determine chemical exchange rates (18–20). One of these other methods, the ‘omega plot’ method, is identical to the Hanes calibration method [eqn (3)], but with two exceptions (20). The Hanes method assumes that MR saturation is instantaneous and complete (where $k_{ex} \ll \omega_1$, and ω_1 is the saturation power). This assumption was satisfactory for the amine of Yb-DO3A-oAA for all but the highest-studied temperatures, but not for the amide for all but the lowest-studied temperatures. The omega plot method assumes that the T_{1sat} relaxation of the agent, r_{1sat}[CA], is negligible. This assumption was satisfactory for the previously reported study of 20 mM of Eu(III) chelates using omega plots because the r_{1sat} relaxivities of Eu(III) chelates are extremely low. This assumption is not satisfactory for 20 mM of Yb-DO3A-oAA that has non-negligible r_{1sat} relaxivities. Therefore, care must be taken to select the most appropriate method for each CEST agent when studying chemical exchange rates.

Finally, this study establishes that a self-calibrating PARACEST agent can more definitively detect enzyme activity relative to other enzyme-responsive PARACEST agents. If the CEST effect of the responsive amine is detected, regardless of the detection of the control amide's CEST effect, then this result is conclusive proof that active esterases are present (assuming that the agent is specific for esterases). If only the CEST effect of the control amide is detected, then this result is conclusive proof that active esterases are not present (at physiological pH and temperature, and waiting sufficiently long for catalysis of enough agent for detection). If both CEST effects are absent, then this result is conclusive proof that the combination of concentration, temperature, pH and T_{1W} relaxation time is inappropriate for detecting esterase activity with this PARACEST agent. The latter two conclusions cannot be reached with a PARACEST agent that has a single enzyme-responsive CEST effect. Therefore, this self-calibrating PARACEST agent can more definitively detect enzyme activity relative to other enzyme-responsive PARACEST agents.

A PARACEST MRI contrast agent that detects esterase enzyme activity may have utility for detecting the delivery of drug nanocarriers to esterase-rich endosomes within pathological tissues, or for detecting esterase-dependent pathologies such as some liver diseases and infections (such as infections of *P. aeruginosa*) (13,21,22). However, esterases are also present in plasma, which will require an esterase-responsive PARACEST agent to be protected during i.v. delivery to pathological tissues (23). Millimolar concentrations are required for adequate CEST detection from this PARACEST agent, which exacerbates concerns regarding delivery and toxicity (7).

As an alternative, the ester group of the tri-methyl lock is a modular 'trigger' that can be replaced by a phosphate group. Cleavage by a phosphatase enzyme may trigger lactonization of the tri-methyl lock moiety and formation of Yb-DO3A-oAA (24). As another alternative, the phenylester can be replaced with a quinone, which can then be reduced to a hydroquinone that can trigger lactonization (25). Yet delivery and toxicity of phosphatase-responsive and redox-responsive PARACEST agents may still be problematic. Additional studies are warranted to test these alternative triggers and evaluate delivery and toxicity issues before this type of enzyme-responsive PARACEST agent is used for pre-clinical studies or clinical diagnoses. More generally, MRI with PARACEST agents must overcome other daunting hurdles before *in vivo* imaging can be routinely achieved, including complications from the competing magnetization transfer effect, slow temporal resolution of CEST MRI acquisition methods, greater MR coalescence at lower magnetic field strengths that are typically used for clinical imaging, and potential tissue heating during the saturation period (3,26).

4. Conclusions

The PARACEST MRI contrast agent, Yb-DO3A-oAA-TML-ester, detected esterase enzyme activity in solution and in cell culture medium by generating an enzyme-responsive CEST effect that was compared with a control CEST effect from the same agent. The ratio of these two CEST effects was independent of concentration and T_1 relaxation, which demonstrated that the agent is self-calibrating and can detect enzyme activity without concern for these factors. High chemical exchange rates can lead to incomplete saturation, so that a simplistic ratiometric comparison of the two CEST effects should be conducted at constant temperature. However, the ratio of concentrations of the saturated amide and saturated amine were constant throughout a wide temperature range, which demonstrated that the agent is self-calibrating especially under physiological conditions. The two CEST effects also showed evidence of having different pH dependencies, so that this agent was not self-calibrating with respect to pH.

5. Experimental

5.1. Synthesis

DO3A-oAA was synthesized in four steps (Fig. 2). Briefly, 1.5 equivalents (4.38 g, 21.72 mmol) of 2-bromoacetyl bromide in 10 ml $CHCl_3$ was added dropwise to 2.00 g (14.48 mmol) of 2-nitrobenzenamine in 50 ml $CHCl_3$. After adding 1.5 equivalents (21.72 mmol) of triethylamine, the reaction was stirred for 1 h at 0°C, and then stirred for an additional 0.5 h at room temperature. The reaction mixture was washed with 10 ml of 5% aqueous $NaHCO_3$ three times. To remove residual water, 10 g of Na_2SO_4 was added to form an insoluble adduct with water that was removed by filtration. The $CHCl_3$ solvent was removed by rotary evaporation. A 200–400 mesh silica gel chromatographic column was used to obtain the product with quantitative purity by using a 1:4 mixture of ethyl acetate and petroleum ether. The total yield of **1** from these initial steps was 50%. To continue the synthesis, 1.00 g (3.87 mmol) of **1** was mixed with 0.7 equivalents (2.71 mmol) of DO3A-t-Bu-ester and 6 equivalents (23.22 mmol) of K_2CO_3 in 100 ml acetonitrile. The mixture was heated at 70 °C for 24 h. The product **2** was purified with a 200–400 mesh silica gel chromatographic column to obtain quantitative purity by using a 1:19 mixture of methanol and ether. The resulting yield was 80%. The protecting groups in **2** were then removed by dissolving 0.81 mmol of **2** in 10 ml TFA for 6 h with a yield of 98%. After removing TFA through rotary evaporation, the product was dissolved in ~1 ml of methanol and added dropwise to ether to form a precipitation. This methanol/ether precipitation process was repeated two additional times to further purify the product. The nitro group in **3** was reduced to an amine group by hydrogenation with 10% Pd/C catalyst in 20 ml water and 3 atm H_2 gas for 24 h (Series 3911 hydrogenator, Parr Instruments Inc.). The final product **4** was lyophilized to obtain a yield of 90% from this final step. The structure of DO3A-oAA was confirmed with ^1H NMR spectroscopy performed at 600 MHz magnetic field strength at room temperature, in 99.9% D_2O solvent, and referenced to the residual H_2O resonance at 4.8 ppm [δ 2.54 (s, 2H), 2.78 (b, 6H), 3.34 (b, 16H), 5.98 (s, 1H), 7.37(t, 1H), 7.76 (t, 1H), 8.07 (d, 2H), 9.60 (s, 1H)] and mass spectroscopy {MALDI-MS *m/z*: 495.3 (calcd 494.25) $[C_{22}H_{36}N_6O_7 + H]^+$}.

Yb-DO3AA-oAA was prepared by mixing 300 mg of **4** and $YbCl_3$ at a molar ratio of 1:1.01, in pH 6 aqueous solution at 60 °C for 2 h. The pH was increased to 8.0 by dropwise addition of 1 M NaOH for an additional 0.5 h. After precipitating the excess free Yb(III) ions by adjusting the pH to 12, the solution was centrifuged, filtered and lyophilized. The concentrations of **5** were determined by ICP MS analysis. Although the final product contained Na^+ and Cl^- ions, this salt did not affect subsequent studies. The composition of **5** was confirmed with mass spectroscopy {ESI-MS *m/z*: 688.2 (calcd 688.2) $[C_{22}H_{31}N_6O_7Yb + Na]^+$}.

TML-ester [3-(2′-acetoxy-4′,6′-dimethylphenyl)-3,3-dimethyl-propionic acid] was synthesized using a previously reported procedure (12). The structure of TML-ester was confirmed with ^{1}H NMR spectroscopy ($CDCl_3$) {δ 1.61 [6H, s, 3-$(CH_3)_2$], 2.26 (3H, s, 6′-CH_3), 2.31 (3H, s, acetyl-CH_3), 2.57 (3H, s, 4′-CH_3), 2.87 (2H, s, 2-CH_2), 6.64, 6.85 (2H, 2s, ArH) and mass spectroscopy (ESI-MS *m/z*: 265.14 (calcd 264.9) $[C_{15}H_{21}O_4]^+$}.

Yb-DO3A-oAA and TML-ester were coupled with an amide bond to form Yb-DO3A-OAA-TML-ester (Fig. 2). TML-ester (0.5 g, 1.88 mmol) was dissolved in a 20 ml of a 1:1 mixture of dry pyridine–DMF at room temperature under argon and treated with EDCI (0.36 g, 1.88 mmol). After stirring the resulting solution at room temperature for 1.5 h, **5** (0.4 g, 0.6 mmol) was added and the reaction mixture was stirred at room temperature for 48 h under argon gas. The reaction mixture was treated with 100 ml of EtOAc and washed with water. The water layer was concentrated to dryness using lyophilization. The white residue was purified using HPLC to obtain quantitative purity [Aliance HPLC system with a C18 column for peptides (Waters Corp.); **6** eluted at 26.9 min during a solvent gradient of 0–30% acetonitrile over 41 min]. A total of 210 mg (0.228 mmol) of **6** was obtained, which represented a 38% yield. The composition of **6** was confirmed with mass spectroscopy {ESI-MS *m/z*: 934.3 (calcd 934.2) $[C_{22}H_{31}N_6O_7Yb + Na]^+ = 934.2$}.

5.2. Detection of esterase enzyme activity

A total of 25 mM of Yb-DO3A-oAA-TML-ester was added to 617 nM of porcine liver esterase (Chemicon, Inc.) at 25 °C and pH 7.4 in phosphate buffer. This concentration of esterase represented 3 units of this enzyme, for which 1 unit catalyzes 1.0 μmol of an ester per minute at pH 8.0 at 25 °C. (27). CEST studies were conducted before and 24 h after combining the contrast agent and esterase using the same CEST measurement protocol listed in section 5.3. The pH was measured using a microelectrode immediately before each CEST study.

Approximately 10^9 cells ml^{-1} of PA10145-U *P. aeruginosa* bacterial cells were cultured overnight in 45 ml of sterile, autoclaved lysogeny broth medium. This medium was collected, passed through a 0.2 μm filter and autoclaved for 30 min at 121 °C. This process was repeated without autoclaving the medium after filtering. Each type of medium was used to create a 25 mM solution of Yb-DO3A-oAA-TML-ester. CEST studies were conducted immediately after creating each solution and after incubating the sample at 25 °C for 24 h using the same CEST measurement protocol listed below. The pH was measured using a microelectrode immediately before each CEST study.

5.3. CEST measurements

CEST MR studies were conducted using a 600 MHz Varian Inova NMR spectrometer. Unless otherwise noted, each sample was tested at 20 mM concentration, 37 °C and pH 7.2 in a phosphate buffer. The pH of the 20 mM stock solution was measured with a calibrated pH microelectrode. The temperature of a NMR sample in the spectrometer was calibrated using a sealed sample of pure ethylene glycol. The concentration of the 20 mM stock solution of the contrast agent was verified using ICP-MS to measure lanthanide content. Concentration-dependent studies were conducted by serially diluting the 20 mM solution to

15, 10, 9.5, 7, and 3 mM with a calibrated pipette, and using the same phosphate buffer. The CEST measurement of the amine at 3 mM concentration was unexpectedly very low, presumably due to poor Lorentzian line fitting, and was not included in the analysis. The T_{1W} relaxation-dependent studies were conducted by serially adding 2–3 μl of 2.5 mM gadodiamide (Omniscan™, GE Healthcare Inc.) to a 200 μl sample of the agent, without correcting for minor dilution of the contrast agent. The T_{1W} values of these doped samples ranged from 1.42 to 0.74 s.

A standard pulse-acquire NMR protocol was prepended with 3.0 s of continuous-wave radio frequency saturation at a power of 14.8 μT, which was sufficient to reach steady-state saturation (7). A total of 32 transients were performed prior to data acquisition to ensure steady-state conditions, and then four transients were acquired at each saturation frequency. The saturation frequencies ranged from +30 to −30 ppm in 1 ppm increments, relative to the chemical shift of water that was referenced to 0 ppm. The resulting 1D NMR spectra were apodized with 20 Hz line broadening, and the amplitude of the water signal was plotted with respect to saturation frequency to obtain a CEST spectrum. A single function that consisted of a sum of three Lorentzian lineshapes was fit to each CEST spectrum using custom routines written for Matlab R2009B (Mathworks Inc., Natick, MA, USA) (Fig. 4). The lineshapes were initially centered at −10, 0 and +12 ppm, and the heights and widths of these lineshapes were initially set to values that were lower than the final values after fitting. A Levenberg–Marquardt least squares fitting routine was used to optimize the fitting of the function to the experimental data, until the iterative change in the function was less than 10^{-20}. The center, width, and amplitude of each Lorentzian line was allowed to change to optimize the fit.

5.4. T_1 relaxation measurements

A T_1 inversion-recovery NMR protocol was used to measure T_1 and T_{1sat} relaxation times. The durations of high-power 180 and 90° excitation pulses were determined using a pulse-acquire NMR protocol. Selective saturation was applied during the relaxation delay and inversion-recovery delay (the delay between the 180 and 90° pulses) at a 14.8 μT power level. The relaxation delay was set to 10 s and eight inversion-recovery delays between 0.2 and 10.0 s were tested. The resulting 1D NMR spectra were apodized with 5 Hz of line broadening, and the amplitude of the water signal was plotted with respect to the inversion-recovery delay. To calculate the T_1 or T_{1sat} relaxation time, the data were fitted to a monoexponential function with a constant to account for a possible DC offset using VNMR (Varian Inc.).

Acknowledgments

This work was supported by the Arizona Cancer Center, the Case Center for Imaging Research and the National Cancer Institute under grants R24CA110943 and R21CA133455-01. V.R.S. was supported through the US Army Medical Research and Materiel Command under grant no. W81XWH-08-BCRP-PREDOC and in part by NIH T32 GM007250. The authors thank Dr Josef Vagner for access to HPLC instrumentation, and thank Dr Walther Ellis and Miriam Eaton for medium from *P. aeruginosa* cultures.

References

1. Zhang S, Merritt M, Woesner DE, Lenkinski RE, Sherry AD. PARA-CEST agents: modulating MRI contrast via water proton exchange. Acc Chem Res. 2003; 36(10):783–790. [PubMed: 14567712]
2. Yoo B, Pagel MD. An overview of responsive MRI contrast agents for molecular imaging. Front Bioscience. 2008; 13:1733–1752.
3. Ali MM, Liu G, Shah T, Flask CA, Pagel MD. Using two chemical exchange saturation transfer magnetic resonance imaging contrast agents for molecular imaging studies. Acc Chem Res. 2009; 42(7):915–924. [PubMed: 19514717]
4. Ward KM, Balaban RS. Determination of pH using water protons and chemical exchange dependent saturation transfer (CEST). Magn Reson Med. 2000; 44(5):799–802. [PubMed: 11064415]
5. Aime S, Barge A, Delli Castelli D, Fedeli F, Mortillaro A, Nielsen FU, Terreno E. Paramagnetic lanthanide(III) complexes as pH-sensitive chemical exchange saturation transfer (CEST) contrast agents for MRI applications. Magn Reson Med. 2002; 47:639–648. [PubMed: 11948724]
6. Yoo B, Raam M, Rosenblum R, Pagel MD. Enzyme-responsive PARACEST MRI contrast agents: A new biomedical imaging approach for studies of the proteasome. Contrast Media Mol Imag. 2007; 2:189–198.
7. Liu G, Lu Y, Pagel MD. Design and characterization of new irreversible responsive PARACEST MRI contrast agent that detects nitric oxide. Magn Reson Med. 2007; 58:1249–1256. [PubMed: 18046705]
8. Terreno E, Delli Castelli D, Cravotto G, Milone L, Aime S. Ln(III)-DOTAMGly complexes: a versatile series to assess the determinants of the efficacy of paramagnetic chemical exchange saturation transfer agents for magnetic resonance imaging applications. Invest Radiol. 2004; 39:235–243. [PubMed: 15021328]
9. Yoo B, Pagel MD. A PARACEST MRI contrast agent to detect enzyme activity. J Am Chem Soc. 2006; 128:14032–14033. [PubMed: 17061878]
10. Chauvin T, Durand P, Bernier M, Meudal H, Doan BT, Noury F, Badet B, Beloeil JC, Tóth E. Detection of enzymatic activity by PARACEST MRI: a general approach to target a large variety of enzymes. Angew Chem Int Ed. 2008; 47(23):4370–4372.
11. Amsberry KL, Gerstenberger AE, Borchardt RT. Amine prodrugs which utilize hydroxy amide lactonization. II. A potential esterase-sensitive amide prodrug. Pharm Res. 1991; 8(4):455–461. [PubMed: 1871039]
12. Henkelman RM, Huang X, Xiang QS, Stanisz GJ, Swanson SD, Bronskill MJ. Quantitative interpretation of magnetization transfer. Magn Reson Med. 1993; 29(6):759–766. [PubMed: 8350718]
13. Picard B, Denamur E, Barakat A, Elion J, Goullet P. Genetic heterogeneity of Pseudomonas aeruginosa clinical isolates revealed by esterase electrophoretic polymorphism and restriction fragment length polymorphism of the ribosomal RNA gene region. J Med Microbiol. 1994; 40(5): 313–322. [PubMed: 7909849]
14. Mann BE. The application of the ForsCn–Hoffman spin-saturation method of measuring rates of exchange to the ^{13}C NMR spectrum of IV&V-dimethylformamide. J Magn Reson. 1977; 25:91–94.
15. Ernst, RR.; Bodenhausen, G.; Wokaun, A. International Series of Monographs on Chemistry. Oxford University Press; Oxford: 1987. Principles of Nuclear Magnetic Resonance in One and Two Dimensions.
16. Woessner DE, Zhang S, Merritt ME, Sherry AD. Numerical solution of the Bloch equations provides insights into the optimum design of PARACEST agents for MRI. Magn Reson Med. 2005; 53:790–799. [PubMed: 15799055]
17. Liepinsh E, Otting G. Proton exchange rates from amino acid side chains-implications for image contrast. Magn Reson Med. 1996; 35:30–42. [PubMed: 8771020]
18. McMahon MT, Gilad AA, Zhou J, Sun PZ, Bulte JWM, van Zijl PCM. Quantifying exchange rates in chemical exchange saturation transfer agents using the saturation time and saturation power dependencies of the magnetization transfer effects on the magnetic resonance imaging signal

(QUEST and QUESP): pH calibration for poly-l-lysine and a starburst dendrimer. Magn Reson Med. 2006; 55:836–847. [PubMed: 16506187]

19. Zhou J, Wilson DA, Sun PZ, Klaus JA, van Zijl PCM. Quantitative description of proton exchange processes between water and endogenous and exogenous agents for WEX, CEST, and APT experiments. Magn Reson Med. 2004; 49:998–1005.
20. Dixon TW, Ren J, Lubag AJ, Ratnakar J, Vinogradov E, Hancu I, Lenkinski RE, Sherry AD. A concentration-independent method to measure exchange rates in PARACEST agents. Magn Reson Med. 2010; 63:625–632. [PubMed: 20187174]
21. Barrett, AJ. Lysosomal enzymes. In: Dingle, JT., editor. Lysosomes. North-Holland: Amsterdam; 1972. p. 46-135.
22. Ross MK, Crow JA. Human carboxylesterases and their role in xenobiotic and endobiotic metabolism. J Biochem Mol Toxicol. 2007; 21(4):187–196. [PubMed: 17936933]
23. La Du B. Plasma esterase activity and the metabolism of drugs with ester groups. Ann NY Acad Sci. 1971; 179:684–694. [PubMed: 4936783]
24. Ueda Y, Mikkilineni AB, Knipe JO, Rose WC, Casazza AM, Vyas DM. Novel water soluble phosphate prodrugs of Taxol® possessing in vivo antitumor activity. Bioorg Med Chem Lett. 1993; 3(8):1761–1766.
25. Amsberry KL, Borchardt RT. Amine prodrugs which utilize hydroxy amide lactonization. II. A potential redox-sensitive amide prodrug. Pharm Res. 1991; 8(3):323–330. [PubMed: 2052518]
26. Liu G, Ali M, Yoo B, Griswold MA, Tkach JA, Pagel MD. PARACEST MRI with improved temporal resolution. Magn Reson Med. 2009; 61(2):399–408. [PubMed: 19165903]
27. Adler AJ, Kistiakowsky GB. Kinetics of pig liver esterase catalysis. J Am Chem Soc. 1962; 84(5): 695–703.

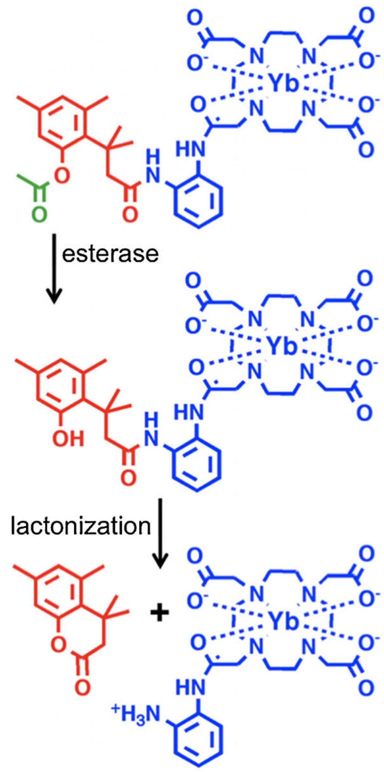

Figure 1.

The mechanism of esterase enzyme detection. After the ester (green) is cleaved by an esterase enzyme, the tri-methyl lock moiety (red) can undergo lactonization to form a hydrocourmarin and also convert an amide to an amine in the Yb-DO3A-oAA PARACEST MRI contrast agent (blue). The appearance of the CEST effect from this amine is used to detect esterase enzyme activity. The CEST effect of the amide of Yb-DO3A-oAA is used as an internal control.

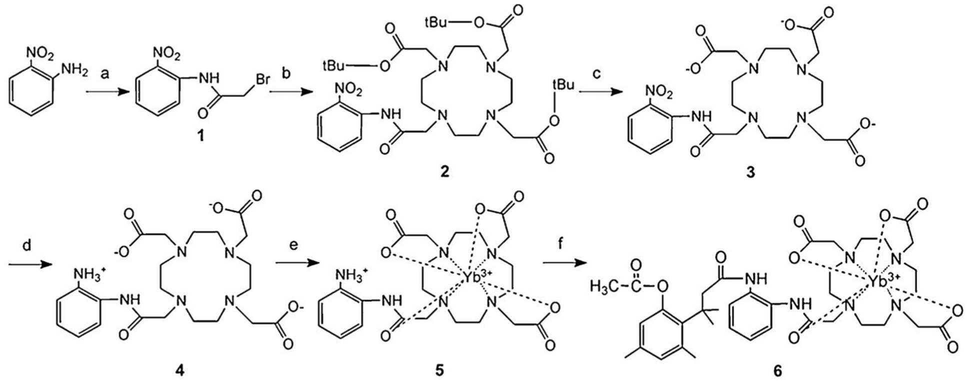

Figure 2.

Synthesis of Yb-DO3A-oAA-TML-ester: (a) 2-bromoacetyl bromide (1.5 equiv.), $(CH_2CH_3)_3N$ (1.5 equiv.), $CHCl_3$, 0 °C, 1 h, r.t., for 30 min, 50%; (b) DO3A-t-Bu-ester (0.7 equiv.), K_2CO_3 (6 equiv.), acetonitrile, 70 °C, 24 h, 80%; (c) 100% TFA, 6 h, 98%; (d) Pd–C (10%), water, H_2 (3 atm), 90%; (e) $YbCl_3$, water (pH 6.0), 60 °C, 2 h, 90%; (f) TML-ester [3-(2′-acetoxy-4′,6′-dimethylphenyl)-3,3-dimethylpropionic acid], EDCl, py/DMF, r.t., 48 h, 38%.

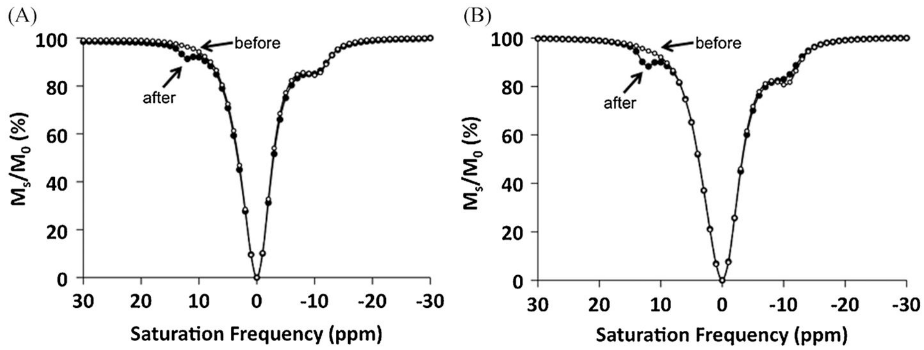

Figure 3.

Detection of esterase enzyme activity with a PARACEST agent. Before enzyme catalysis, the control CEST effect was present at −10 ppm (solid circles). The enzyme-responsive CEST effect appeared at 12 ppm (open circles) after (A) adding esterase to 20 mM of Yb-DO3A-oAA-TML-ester, and (B) after incubation of 20 mM of Yb-DO3A-oAA-TML-ester in medium used to culture *P. aeruginosa*. In both cases, the control CEST effect at −10 ppm was unaffected by the esterase enzymes except for a small decrease in CEST that was attributed to a lower pH of the sample that occurred during de-esterification. Data points are connected by a line to aid visualization of the results, and the line does not represent the Lorentzian lineshapes that were used in the analyses.

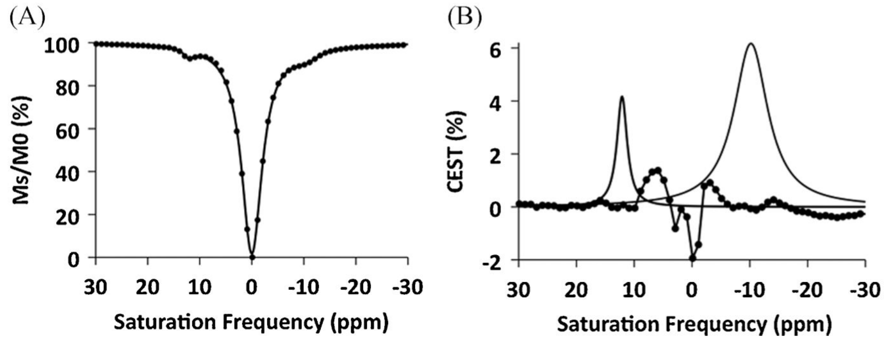

Figure 4.

Lorentzian line-fitting of a CEST spectrum. (A) A single function that consisted of a sum of three Lorentzian lines (solid line) was fit to the experimental data (solid circles) for a CEST spectrum of 7 mM of Yb-DO3A-oAA. Similar results were obtained from fitting other CEST spectra. (B) The residuals of the fitting routine (experimental data – fitted result, shown as solid circles connected with a line) were negligible near the peaks of the fitted Lorentzian lines for the CEST effects of the amine and amide (shown as solid lines that are peaked at +12 and −10 ppm, respectively).

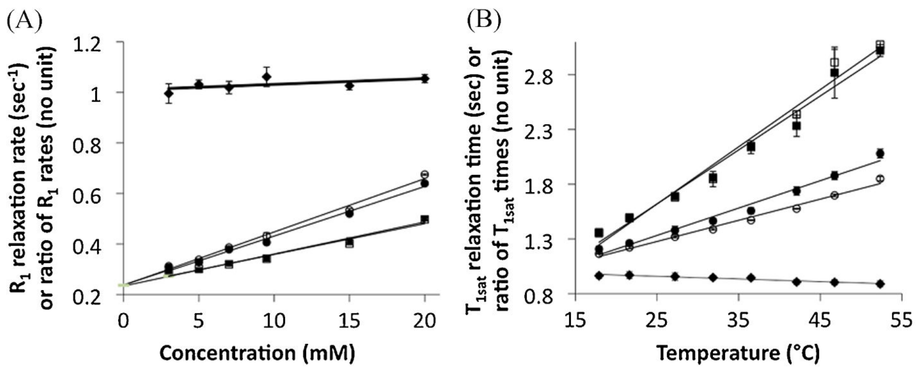

Figure 5.

The T_1 relaxation properties of Yb-DO3A-oAA. Results are shown with respect to (A) concentration and (B) temperature for selective saturation of the amide (solid circles) and amine (open circles), and for control studies with no saturation (solid squares) and selective saturation at +80 ppm (open squares). These linear relationships have an r^2 correlation coefficient > 0.98. The amine-to-amide ratio is also shown (solid diamonds). Error bars represent the standard deviation of the T_1 inversion-recovery data fitting routine, and are smaller than the symbol for many data points. The concentration-dependent ratio of R_{1sat} relaxation rates is relatively constant compared with the rates of the amine or amide.

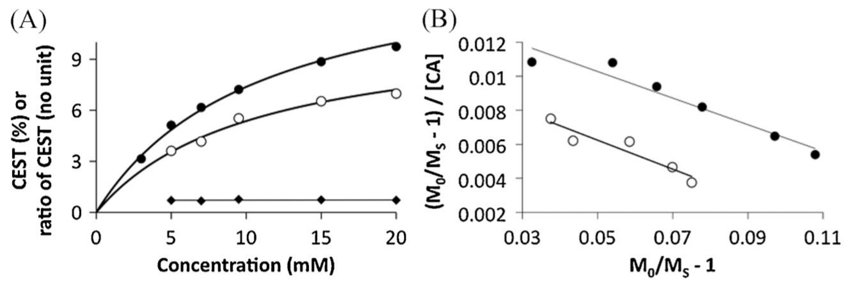

Figure 6.

The dependence of the CEST effect of Yb-DO3A-oAA on concentration for the amide (solid circles) and amine (open circles). (A) The CEST effects of the amine and the amide of Yb-DO3A-oAA each increased with increasing concentration, but the ratio of the CEST effects was insensitive to changes in concentration. (B) The Hanes calibration [eqn (4)] was used to measure the r_{1sat} relaxivities and chemical exchange rates of the agent, and the linearities of each calibration confirmed that the chemical exchange of the amide and amine are sufficiently described by a two-pool model.

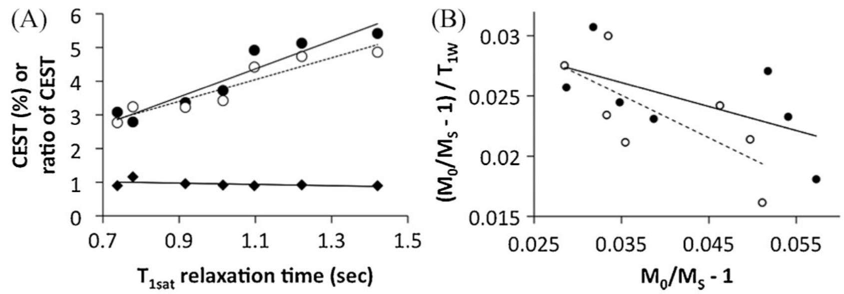

Figure 7.

(A) The dependence of the CEST effect of Yb-DO3A-oAA on T_{1W} relaxation times for the amide (solid circles, solid line) and amine (open circles, dashed line). (B) The slope and *y*-intercept of a modification of the Hanes calibration separates the conditions of concentration and chemical exchange rate (k_{ex}), respectively. The r^2 correlation coefficient is 0.50 and 0.36 for the calibration of the amine and amide, respectively.

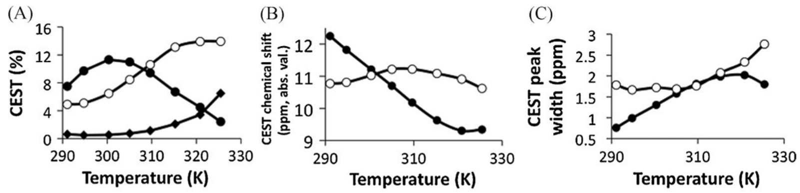

Figure 8.

The dependence of the CEST effect of Yb-DO3A-oAA on temperature for the amide (solid circles) and amine (open circles) and the amine-to-amide ratio (solid diamonds). Lines that connect the data points are provided as a visual aid. (A) The decreasing CEST effect of the amide with increasing temperatures reflects chemical shift coalescence that leads to incomplete saturation. The plateau of the amine's CEST effect also indicates evidence for chemical shift coalescence at the highest temperatures. The ratio of the CEST effects is also dependent on temperature, but to a lesser extent especially at or below physiological temperatures (310 K). (B) The chemical shifts of the CEST effects depend on temperature. The absolute value of the chemical shifts is shown to facilitate visualization on one graph. (C) An increase in the CEST peak widths of the amide and amide indicates an increasing chemical exchange rate with increasing temperature (except for the amide at the highest temperature).

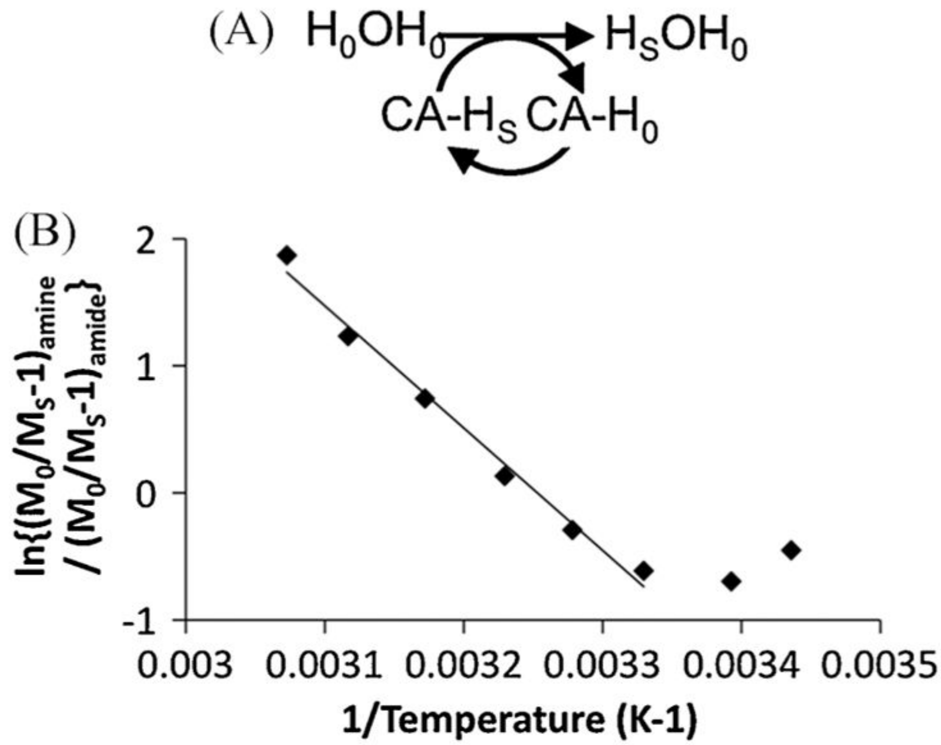

Figure 9.

A more sophisticated analysis of the dependence of the CEST effect of Yb-DO3A-oAA on temperature. (A) The CEST effect is considered to be a first-order chemical reaction in which the PARACEST agent acts as a catalyst. (B) The plot of eqn (7) shows a linear relationship between 27.2 and 53.2 °C, indicating that the ratio of concentrations of the saturated amine and amide is constant within this temperature range.

Table 1

MR parameters and experimental measurements for Yb-DO3A-oAA

Chemical group	Saturation frequency	r_{1sat} relaxivity or r_1 relaxivity	T_{1sat}/temperature	$-r_{1sat}T_{1W}$		k_{ex}	$n_{CA}k_{ex}$
				CEST analysis	T_1 relaxation analysis		
Amine	+12 ppm	0.0211 mM^{-1} s^{-1}	0.019 s° C^{-1}	−0.0852 mM^{-1}	−0.0890 mM^{-1}	93 Hz	279 Hz
Amide	−10 ppm	0.0194 mM^{-1} s^{-1}	0.025 s° C^{-1}	−0.0782 mM^{-1}	−0.0819 mM^{-1}	375 Hz	375 Hz
Amine/amide	—	1.06	0.0024	1.089	1.086	0.24	0.74
Control	+80 ppm	0.0126 mM^{-1} s^{-1}	—	—	—	—	—
Control	No saturation	0.0121 mM^{-1} s^{-1}	—	—	—	—	—